52

SATELLITE & MESOMETEOROLOGY RESEARCH PROJECT

Department of the Geophysical Sciences
The University of Chicago

STABILITY AND DIFFERENTIAL ADVECTION ASSOCIATED WITH TORNADO DEVELOPMENT

by

Tetsuya Fujita and Dorothy L. Bradbury

(Chapter VI of a Comprehensive Study of the Palm Sunday Tornadoes, 1965)

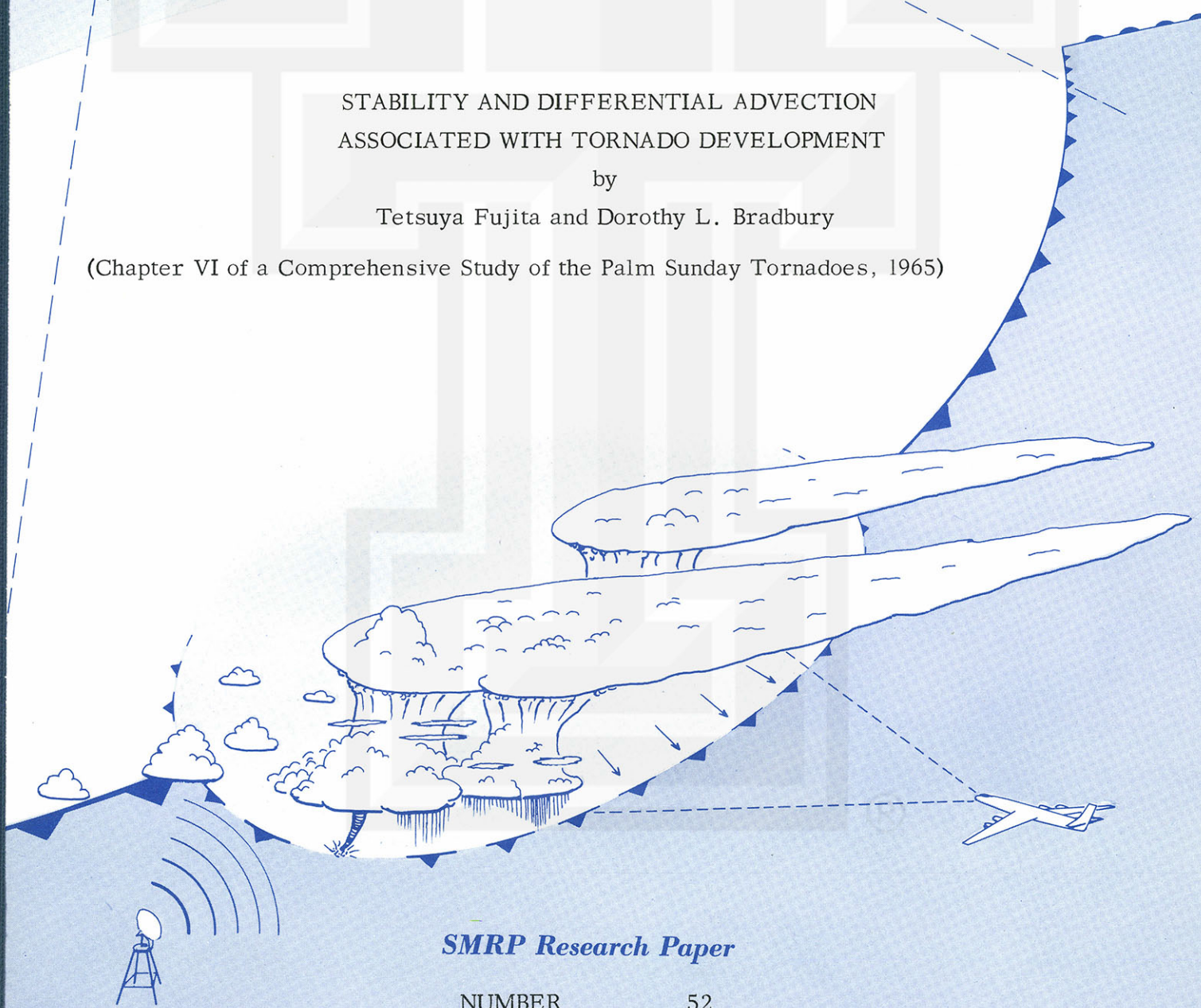

SMRP Research Paper

NUMBER 52

March 1966

MESOMETEOROLOGY PROJECT --- RESEARCH PAPERS

1.* Report on the Chicago Tornado of March 4, 1961 - Rodger A. Brown and Tetsuya Fujita

2.* Index to the NSSP Surface Network - Tetsuya Fujita

3.* Outline of a Technique for Precise Rectification of Satellite Cloud Photographs - Tetsuya Fujita

4.* Horizontal Structure of Mountain Winds - Henry A. Brown

5.* An Investigation of Developmental Processes of the Wake Depression Through Excess Pressure Analysis of Nocturnal Showers - Joseph L. Goldman

6.* Precipitation in the 1960 Flagstaff Mesometeorological Network - Kenneth A. Styber

7.** On a Method of Single- and Dual-Image Photogrammetry of Panoramic Aerial Photographs - Tetsuya Fujita

8. A Review of Researches on Analytical Mesometeorology - Tetsuya Fujita

9. Meteorological Interpretations of Convective Nephsystems Appearing in TIROS Cloud Photographs - Tetsuya Fujita, Toshimitsu Ushijima, William A. Hass, and George T. Dellert, Jr.

10. Study of the Development of Prefrontal Squall-Systems Using NSSP Network Data - Joseph L. Goldman

11. Analysis of Selected Aircraft Data from NSSP Operation, 1962 - Tetsuya Fujita

12. Study of a Long Condensation Trail Photographed by TIROS I - Toshimitsu Ushijima

13. A Technique for Precise Analysis of Satellite Data; Volume I - Photogrammetry (Published as MSL Report No. 14) - Tetsuya Fujita

14. Investigation of a Summer Jet Stream Using TIROS and Aerological Data - Kozo Ninomiya

15. Outline of a Theory and Examples for Precise Analysis of Satellite Radiation Data - Tetsuya Fujita

16. Preliminary Result of Analysis of the Cumulonimbus Cloud of April 21, 1961 - Tetsuya Fujita and James Arnold

17. A Technique for Precise Analysis of Satellite Photographs - Tetsuya Fujita

18. Evaluation of Limb Darkening from TIROS III Radiation Data - S.H.H. Larsen, Tetsuya Fujita, and W.L. Fletcher

19. Synoptic Interpretation of TIROS III Measurements of Infrared Radiation - Finn Pedersen and Tetsuya Fujita

20. TIROS III Measurements of Terrestrial Radiation and Reflected and Scattered Solar Radiation - S.H.H. Larsen, Tetsuya Fujita, and W.L. Fletcher

21. On the Low-level Structure of a Squall Line - Henry A. Brown

22. Thunderstorms and the Low-level Jet - William D. Bonner

23. The Mesoanalysis of an Organized Convective System - Henry A. Brown

24. Preliminary Radar and Photogrammetric Study of the Illinois Tornadoes of April 17 and 22, 1963 - Joseph L. Goldman and Tetsuya Fujita

25. Use of TIROS Pictures for Studies of the Internal Structure of Tropical Storms - Tetsuya Fujita with Rectified Pictures from TIROS I Orbit 125, R/O 128 - Toshimitsu Ushijima

26. An Experiment in the Determination of Geostrophic and Isallobaric Winds from NSSP Pressure Data - William Bonner

27. Proposed Mechanism of Hook Echo Formation - Tetsuya Fujita with a Preliminary Mesosynoptic Analysis of Tornado Cyclone Case of May 26, 1963 - Tetsuya Fujita and Robbi Stuhmer

28. The Decaying Stage of Hurricane Anna of July 1961 as Portrayed by TIROS Cloud Photographs and Infrared Radiation from the Top of the Storm - Tetsuya Fujita and James Arnold

29. A Technique for Precise Analysis of Satellite Data, Volume II - Radiation Analysis, Section 6. Fixed-Position Scanning - Tetsuya Fujita

30. Evaluation of Errors in the Graphical Rectification of Satellite Photographs - Tetsuya Fujita

31. Tables of Scan Nadir and Horizontal Angles - William D. Bonner

32. A Simplified Grid Technique for Determining Scan Lines Generated by the TIROS Scanning Radiometer - James E. Arnold

33. A Study of Cumulus Clouds over the Flagstaff Research Network with the Use of U-2 Photographs - Dorothy L. Bradbury and Tetsuya Fujita

34. The Scanning Printer and Its Application to Detailed Analysis of Satellite Radiation Data - Tetsuya Fujita

35. Synoptic Study of Cold Air Outbreak over the Mediterranean using Satellite Photographs and Radiation Data - Aasmund Rabbe and Tetsuya Fujita

36. Accurate Calibration of Doppler Winds for their use in the Computation of Mesoscale Wind Fields - Tetsuya Fujita

37. Proposed Operation of Intrumented Aircraft for Research on Moisture Fronts and Wake Depressions - Tetsuya Fujita and Dorothy L. Bradbury

38. Statistical and Kinematical Properties of the Low-level Jet Stream - William D. Bonner

39. The Illinois Tornadoes of 17 and 22 April 1963 - Joseph L. Goldman

40. Resolution of the Nimbus High Resolution Infrared Radiometer - Tetsuya Fujita and William R. Bandeen

41. On the Determination of the Exchange Coefficients in Convective Clouds - Rodger A. Brown

* Out of Print
** To be published

(Continued on back cover)

SATELLITE AND MESOMETEOROLOGY RESEARCH PROJECT
Department of the Geophysical Sciences
The University of Chicago

STABILITY AND DIFFERENTIAL ADVECTION ASSOCIATED WITH TORNADO DEVELOPMENT

by
Tetsuya Fujita and Dorothy L. Bradbury

(Chapter VI of a Comprehensive Study of the Palm Sunday Tornadoes, 1965)

SMRP Research Paper #52
March 1966

The research reported in this paper has been supported by the Environmental Science Services Administration under grant Cwb WBG-41.

STABILITY AND DIFFERENTIAL ADVECTION ASSOCIATED WITH TORNADO DEVELOPMENT[1]

Tetsuya Fujita and Dorothy L. Bradbury

Department of the Geophysical Sciences

The University of Chicago

Chicago, Illinois

ABSTRACT

For the purpose of evaluating the usefulness of two parameters, the Best Lifted Index and the Material Differential Advection developed by the authors, the Palm Sunday tornado case was selected. Test analyses revealed that the Best Lifted Index is fairly conservative against the time of day since it automatically excludes high index values resulting from low-level cooling. The areas of specific Best Lifted Index can, therefore, be predicted by advecting them for hours if the movements of other meteorological systems are also known. By expanding conventional Differential Advection, which refers to a fixed location on the earth, a generalized differential advection above the air column moving with either high- or low-level winds has been proposed. This advection, called the Material Differential Advection, gives the rate of change in the lapse rate above horizontally advected air which will rise violently upon reaching the region of steep temperature lapse rate. The Material Differential Advection, when computed while moving with high-level winds, indicates the possibility of initiating strong upward motion in the underlying layers.

1. INTRODUCTION

The thermodynamical and dynamical structure of the atmosphere, which gives rise to the initiation of vigorous thunderstorms, has not yet been fully understood. The thunderstorms forming over the midwestern United States, especially under certain meteorological conditions, are so severe that they overshadow cellular, convective clouds scattered above the heated ground. When an isolated thunderstorm or a group of thunderstorms reaches its mature stage, its mesoscale environment is modified so that small, cellular convective clouds around the major storms are considerably suppressed.

---

[1]The research reported in this paper has been supported by the Environmental Science Services Administration under Weather Bureau grant Cwb WBG-41.

In view of the fact that the circulation of a mature thunderstorm is far from that of a small air parcel rising inside the atmosphere at rest, the use of the so-called "parcel method" should be restricted to small or young clouds which might grow into thunderstorms.

Since the computation of buoyant energy on an adiabatic chart is rather time-consuming for operational purposes, Showalter (1953) proposed a stability index which can be computed from temperature and humidity values on an 850-mb chart and from 500-mb temperatures. The index computation is based upon the parcel method and is made by lifting a parcel at the 850-mb surface dry-adiabatically to saturation and then moist-adiabatically to the 500-mb surface. The algebraic difference between the temperatures of the lifted parcel and its environment is called the Showalter Stability Index (SI), the negative value of which indicates instability. Because the indices are based upon the parcel method, then interpretation on a synoptic map is meaningful only over the region away from thunderstorms. Nevertheless, the areas of the SI above +6C may be regarded as convectively stable, and unusually severe thunderstorm activity may be expected over the region of the SI that is -4C or lower.

The Showalter Stability Index is very easy and quick to compute, since it requires only the 850- and 500-mb charts. Despite this advantage, it occasionally misrepresents the stability of the atmosphere when the source of the moisture to be drawn into a convective cloud is located below the 850-mb surface. When the top of the moist layer is very close to the 850-mb surface, the SI is so sensitive to the height of the moisture top that its interpretation requires a knowledge of the vertical distribution of the moisture below the 850-mb surface.

In order to determine a more realistic stability index based upon the parcel method, Galway (1955) and Winston (1956) proposed the use of a low-level, moist layer for lifting. The SELS unit in Kansas City now uses the mean mixing ratio and the mean potential temperature of the lowest 3000 ft layer as those of the parcel which is lifted to the 500-mb surface, first dry-adiabatically to saturation and then moist-adiabatically. The algebraic difference between the temperatures of the lifted parcel and its environment is called the Lifted Index (LI). The LI can be computed whenever radiosonde data are available below 3000 ft and at 500 mb. Because of the diurnal variation of the air temperature and the mixing ratio within the atmosphere near the surface, it is necessary to forecast the vertical distribution of the air temperature and the mixing ratio for the time of day when the development of severe local storms is predicted. Through this prediction, the atmosphere to be lifted for the LI

computation would represent the thermodynamical characteristics at the time of storm formation several hours later.

From the practical point of view, however, it is rather difficult to predict three parameters--(1) the mean potential temperature of the lowest 3000-ft layer, (2) the mean mixing ratio of the same layer, and (3) the 500-mb temperatures required for the LI computation. The computation of the LI is usually performed on an adiabatic diagram using the forecast surface temperature or the forecast surface potential temperature while keeping both (2) and (3) constant.

2. THE BEST LIFTED INDEX

It has been stated that the Lifted Index for each station at the time of predicted severe storm formation can be computed from the predicted parameters (1), (2), and (3). Parameter (3) is closely related to the 500-mb advection, while (1) and (2) vary because of low-level advection as well as diabatic heating and cooling. The Showalter Index, in fact, is computed without using any predicted values, while the computation of the Lifted Index requires at least the predicted surface temperature.

Because of the difficulty in obtaining a realistic value for the LI representing the stability of the atmosphere at the time of severe storm development, an attempt was made to define a Lifted Index that could be computed from the measured upper-air data without involving short-range forecasting of selected parameters. The field of the indices thus obtained does represent the instability for the upper-air observation times which do not always coincide with the time of storm development. The prediction of the Stability-Index field should be made after the field for the sounding time has been established on the chart. Because of the fact that the 850-mb surface could be higher than the top of a low-level moist layer and that the mean potential temperature of the lowest 3000 ft is strongly affected by the diabatic heating, both the SI and the LI computed from the measured upper-air data either misrepresent the true instability or include significant diurnal variation.

The earth's surface is unique in the sense that the vertical velocity is always zero, allowing vertical motion to increase upward under the influence of a convergent field. This does not mean that a vertical current or updraft should always start from the earth's surface. The inflow air of a nocturnal thunderstorm could be coming from some layer slightly above the cold surface air.

In order to compute easily the Lifted Index as a function of the base of an

updraft, a layer of 50-mb thickness above an arbitrary pressure surface is assumed to represent the inflow layer (figure 1). Two open circles in each 50-mb thickness layer represent the mean mixing ratio and the mean potential temperature plotted on each P-25 mb surface. By lifting the parcel from the P-25 mb surface dry-adiabatically to the condensation level and then moist-adiabatically to 500 mb, a Lifted Index can be obtained. The Lifted Index varies naturally as a function of the pressure (or height) at the base of the updraft. In other words, the Lifted Index varies with the pressure when the base of the updraft is moved upward from the ground. Figure 1 represents the lifting from three surfaces with pressures P_0, P_1, and P_2, of which the lifting from the surface of pressure P_1 gives the lowest Lifted Index or the largest instability.

The lowest Lifted Index obtained by moving the pressure surface from the ground upward is called the Best Lifted Index (BLI). The pressure and the height of the surface used to obtain the BLI are designated as the Pressure of the Best Lifting (PBL) and the Height of the Best Lifting (HBL) respectively.

3. EXAMPLES OF THE BEST LIFTED INDEX AND THE PRESSURE OF THE BEST LIFTING

For the purpose of testing the use and validity of the BLI and the PBL, the meteorological conditions involved in the Palm Sunday tornadoes were analyzed. As has been discussed in Chapters III and IV, the tornadoes occurred in the warm sector to the east of a dry, cold front advancing rapidly across the Midwest. The series of 850-mb charts in figures 2, 4, and 6 represents the advance of the dry, cold front extending from the center of a continental cyclone to Texas. The cyclone moved to the east-northeast at the rate of about 35 kt. The stippled areas with dew-point temperatures above +5C also moved rapidly eastward as the dry, cold front wiped out their western boundaries.

Analyzed in figure 3 are the isolines of the BLI and the PBL computed from the 06 CST soundings on April 11, 1965 about 5 hours prior to the formation of the Palm Sunday tornadoes in Iowa. A tongue of instability characterized by the BLI below -5C is seen along the progressive side of the dry, cold front. To the west of the front the BLI exceeds +10C in some areas. It is of interest to note that the area of the low BLI is included entirely within the region where the PBL represents the surface pressure, indicating that the BLI can be obtained when the lowest 50-mb air is lifted to the 500-mb surface. The figure also includes the winds aloft corresponding to the PBL. These winds are helpful in determining the motion of the air to be lifted from the initial surface.

The BLI and PBL patterns at 18 CST, April 11, 1965 (figure 5) reveal little change in the values of BLI during the 12-hour period. The tongue of instability widened, and a significant gradient of the BLI is seen along the dry, cold front. Tornadoes in progress appear as black circles near the northern tip of the tongue of the low BLI in which the south-southwest winds prevail. The decrease in the PBL or the increase in the HBL is evident to the north of the -5C line where the BLI = 0C line reaches above the 850-mb surface, while the wind directions at the HBL are south or south-southwest. An active, warm-frontal surface can be expected in such an area, since the combination of the PBL and BLI suggests a favorable condition for lifting from a warm-frontal surface. An area of high values of BLI to the west of the dry, cold front is characterized by an extremely dry air mass topped by dry, westerly winds above 700 mb. Advection of high-level moisture near the lower-left corner of the chart resulted in a dome of the HBL. The BLI associated with this moisture advection was so high that no convective activity could be expected there. Most of the area behind the dry, cold front is characterized by a temperature lapse rate of almost isentropic from the ground to near 750 mb. The mixing ratio is quite low. Fujita (Chapter IV) reported dust clouds appeared in the satellite pictures taken on Palm Sunday.

Early Monday morning April 12, 1965 all tornado activity ended, leaving behind some of the worst damage in decades. The BLI and PBL patterns at 06 CST, April 12, 1965 (figure 7) clarify the conditions some 5 hours after the end of the storms.

The patterns of BLI and PBL analysed at 12 hour intervals on April 11 and 12 indicated a remarkable continuity from one chart to the next, suggesting that the prediction of instability regions in the afternoon can be made by using the BLI. When an area of concern is affected by a rapidly moving system such as a dry, cold front, the Lifted Index in the afternoon at a specific location computed from a moving sounding does not always include all advective changes which might take place during the next several hours.

4. LOCAL AND MATERIAL DIFFERENTIAL ADVECTIONS

The term "differential advection" is used to describe a process such that the vertical variation in the horizontal transport of temperature in the atmosphere results in either increase or decrease in the instability of the layer.

Processes of differential advection have been used in earlier studies to explain

the destabilization of the atmosphere to produce severe storms and tornadoes (Whitney and Miller, 1956) and heavy precipitation (Miller, 1955). Crumrine (1965) reported the results of mean differential advection between 850 and 500 mb computed from 15 cases involving severe storm activity. He found that an average differential advection of about 1C per hour is favorable for the development of severe storms when it destabilizes the air mass ahead of an instability line.

The differential advection investigated by these authors deals with the change in the lapse rate between two levels above a given point on the earth. If we express the temperature at a height h_1 by T_1, it can be written as

$$\frac{dT_1}{dt} = \frac{\partial T_1}{\partial t} + \mathbb{V}_1 \cdot \nabla T_1 \qquad (1)$$

The net change in the temperature should be zero since we assume that the processes involved are horizontal advection only. Thus we have

$$\frac{\partial T_1}{\partial t} = - \mathbb{V}_1 \cdot \nabla T_1 \qquad (2)$$

When this is combined with an advective change in temperature at h_2 which is higher than h_1, we obtain the differential advection

$$\frac{\partial (T_2 - T_1)}{\partial t} = \mathbb{V}_1 \cdot \nabla T_1 - \mathbb{V}_2 \cdot \nabla T_2 \qquad (3)$$

This differential advection which is observed above a fixed point on the earth is termed the "Local Differential Advection."

If an observer moves with either upper or lower level wind in order to measure the change in lapse rate along the vertical through the observer, a slightly different differential advection with respect to a moving coordinate system can be obtained. Such a change in the coordinates is meaningful indeed in view of the fact that an atmosphere travels horizontally until a favorable lapse rate for convection is reached. The differential advection thus defined is called the "material differential advection." It should be pointed out that the coordinates may move with either upper- or lower-level winds.

The change in temperature thus observed from a moving coordinate can be written as

$$\frac{\delta T_1}{\delta t} = \frac{\partial T_1}{\partial t} + \mathbb{C} \cdot \nabla T_1 \qquad (4)$$

and

$$\frac{\delta T_2}{\delta t} = \frac{\partial T_2}{\partial t} + \mathbb{C} \cdot \nabla T_2 \qquad (5)$$

where δ is used to designate a variation observed from the coordinates moving with velocity $\mathbb{C}$.

First we assume that the coordinate system moves with the low-level wind, and use the relationships

$$\mathbb{C} = \mathbb{V}_1 , \quad \frac{\delta T_1}{\delta t} = 0 , \quad \frac{\partial T_1}{\partial t} = - \mathbb{V}_1 \cdot \nabla T_1 , \text{ and } \frac{\partial T_2}{\partial t} = - \mathbb{V}_2 \cdot \nabla T_2 \qquad (6)$$

in order to reduce Equations (4) and (5) into

$$\frac{\delta (T_2 - T_1)}{\delta t} = \frac{\partial T_2}{\partial t} - \frac{\partial T_1}{\partial t} = - \mathbb{V}_2 \cdot \nabla T_2 + \mathbb{V}_1 \cdot \nabla T_2 = (\mathbb{V}_1 - \mathbb{V}_2) \cdot \nabla T_2 \qquad (7)$$

$$= - \$ \cdot \nabla T_2 ,$$

where $\$ = \mathbb{V}_2 - \mathbb{V}_1$ denotes the vertical wind shear. This result indicates that the material differential advection when moved with the low-level wind is the inner product of the negative value of the vertical wind shear and the temperature gradient at the upper level.

Next we consider the case in which the coordinate system moves with the upper wind. In this case we know

$$\mathbb{C} = \mathbb{V}_2 , \quad \frac{\delta T_2}{\delta t} = 0 , \quad \frac{\partial T_1}{\partial t} = - \mathbb{V}_1 \cdot \nabla T_1 , \text{ and } \frac{\partial T_2}{\partial t} = - \mathbb{V}_2 \cdot \nabla T_2 \qquad (8)$$

and the Equations (4) and (5) are reduced into

$$\frac{\delta (T_2 - T_1)}{\delta t} = (\mathbb{V}_1 - \mathbb{V}_2) \cdot \nabla T_1 = - \$ \cdot \nabla T_1 . \qquad (9)$$

From these results, the differential advection of temperature can be summarized as

LDA = Local Differential Advection = $\mathbb{V}_1 \cdot \nabla T_1 - \mathbb{V}_2 \cdot \nabla T_2$

MDA-H = Material Differential Advection for high-level wind = $-(\mathbb{V}_2 - \mathbb{V}_1) \cdot \nabla T_1$

MDA-L = Material Differential Advection for low-level wind = $-(\mathbb{V}_2 - \mathbb{V}_1) \cdot \nabla T_2$

These three differential advections abbreviated as LDA, MDA-H, and MDA-L differ from each other. That is, LDA indicates destabilization of the atmosphere above any fixed point on the earth, MDA-H gives destabilization of the atmosphere below an air parcel moving with the high-level wind. MDA-L is for a parcel moving with the low-level wind, which will move upward when the lapse rate inside the overlying air column increases.

5. MATERIAL DIFFERENTIAL ADVECTION IN THE PALM SUNDAY TORNADO CASE, 1965

In order to find out the change in the stability of the atmosphere prior to the time of the Palm Sunday Tornadoes of April 11, 1965, an analysis of the differential advection field was made.

Now we are able to compute three different differential advections referring to the coordinates fixed on the ground (LDA), moving with the high-level wind (MDA-H), and moving with the low-level wind (MDA-L). Under the assumption that the tornado-producing convection started when the warm, moist air from the Gulf of Mexico was advected northward until the lapse rate of the air column above it became so large that violent overturning took place, we moved the coordinates with the 850-mb winds in computing the differential advection. The 700-mb surface was chosen as the upper level for the advection computation, based upon the finding that cold advection was most significant near the top of the dry, cold air mass (Refer to figure 11, Chapter IV by Fujita). The differential advection thus computed represents

$$\text{MDA-L} = -(\mathbb{V}_{700} - \mathbb{V}_{850}) \cdot \nabla T_{700}. \qquad (10)$$

Figure 8 shows the fields of T_{700} and $(\mathbb{V}_{850} - \mathbb{V}_{700})$ and the isolines of MDA-L computed from these fields. The 700-mb isotherms were obtained by smoothing the temperature field analysed over a much larger area. The winds $\mathbb{V}_{850} - \mathbb{V}_{700} = -\$_{850}^{700}$ entered at grid points on the chart were computed from the streamline and isotach field of the vertical wind shear obtained from observed upper winds. The MDA-L contoured for every 1C per 3 hours indicates an area of

negative MDA-L, or of increasing lapse rate over lower Michigan at 06 CST, April 11.

No severe storms were reported in this area of negative MDA-L. When the areas of T_d higher than 50F and of $T_{850} - T_{700}$ higher than 10C were combined with this negative MDA-L area (figure 9), it was found that a small stippled area in the figure satisfies the conditions--large initial lapse rate, high moisture content, and large negative differential advection.

Similar computations were made for 12 CST, but the data used to construct the charts were obtained from only a few observed winds and interpolated isotherm patterns, making the computation of MDA-L very difficult. Nevertheless a small area satisfying the above-mentioned three conditions was located in north central Iowa. It was in this region that the first tornadoes of a series of the Palm Sunday storms were reported around 1230 CST.

At 18 CST the rate of differential advection had increased to a maximum negative value of over -4C per 3 hours (figure 10). The figure reveals that a large negative MDA-L existed along the progressive side of the dry, cold front which was then extended from Lake Michigan to Missouri. The MDA-L behind this front was slightly positive, suggesting that the entire air mass between the 850- and 700-mb surfaces was pushing eastward without noticeable differential advection.

The three parameters were combined in figure 11 to show the locations of tornadoes which were in progress at 18 CST, the map time. More information about these tornadoes appears in Chapter II by Fujita and Chapter V by Bradbury and Fujita. It is of interest to see that all the tornadoes in progress at 18 CST were inside the stippled area which satisfies the three conditions under previous discussion.

6. CONCLUSIONS

A test analysis of the Best Lifted Index proposed by the authors revealed that its diurnal variation is very small, thus permitting us to predict its patterns by simply taking advective factors into consideration. This index is also useful in studying the stability of the air over a warm frontal zone in which the underlying cold air cuts off the moisture supply from low levels from which a parcel should be lifted in order to compute conventional indices.

Proposed and tested herein is the material differential advection which represents the differential advection observed from the coordinates moving with

either high-level or low-level winds. The test analysis revealed that all Palm Sunday Tornadoes at 18 CST, April 11 were located inside the area of large negative values of material differential advection.

REFERENCES

Crumrine, H. A., 1965: The Use of the Horizontal Temperature Advection, the 850-500 mb Thickness, and the 850-500 mb Shear Wind in Severe Local Storms Forecasting. Paper presented at the 244th National Meeting of the American Meteorological Society on Cloud Physics and Severe Local Storms, Oct. 18-22, 1965, Reno, Nevada.

Galway, J. G., 1955: The Lifted Index Predictor of the Showalter Stability Index. Unpublished research report, Severe Local Storm Forecast Center, U. S. Weather Bureau, Kansas City, Mo. 7 pp.

Miller, J. E., 1955: Intensification of Precipitation by Differential Advection. J. Meteor. 12, 472-477.

Showalter, A. K., 1953: A Stability Index for Thunderstorm Forecasting. Bull. Amer. Meteor. Soc., 34, 250-252.

Whitney, L. F. and J. E. Miller, 1956: Destabilization by Differential Advection in the Tornado Situation of 8 June 1963. Bull. Amer. Meteor. Soc., 37, 224-229.

Winston, Jay S., Editor, 1956: Forecasting Guide No. 1, Forecasting Tornadoes and Severe Thunderstorms. Staff Members of Severe Local Storm Forecast Center, U. S. Weather Bureau, Kansas City, Mo. 34 pp.

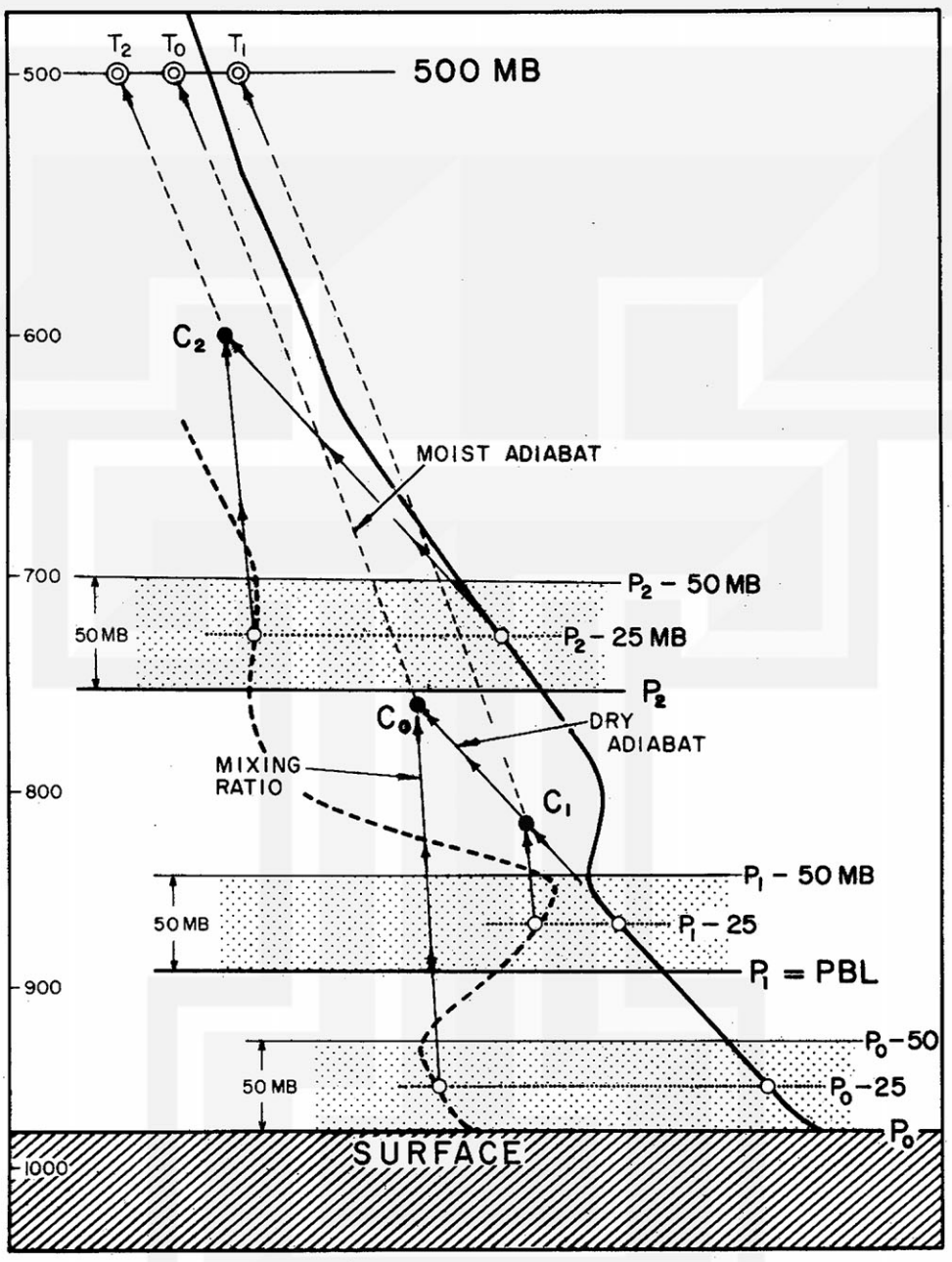

Figure 1. An example of the computation of Pressure of the Best Lifting (PBL) and Best Lifted Index (BLI) on an adiabatic chart.

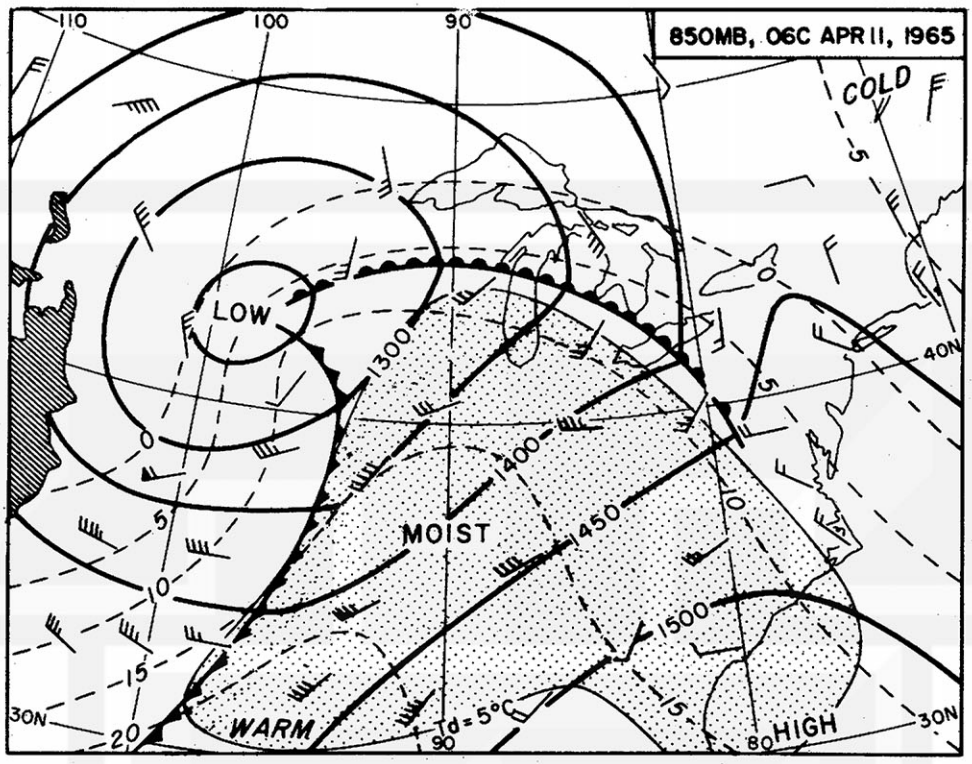

Figure 2. Fronts, contours (solid lines), and isotherms (dashed lines) on the 850-mb surface for 06 CST 11 April 1965. Stippled area represents dewpoint temperatures above 5C.

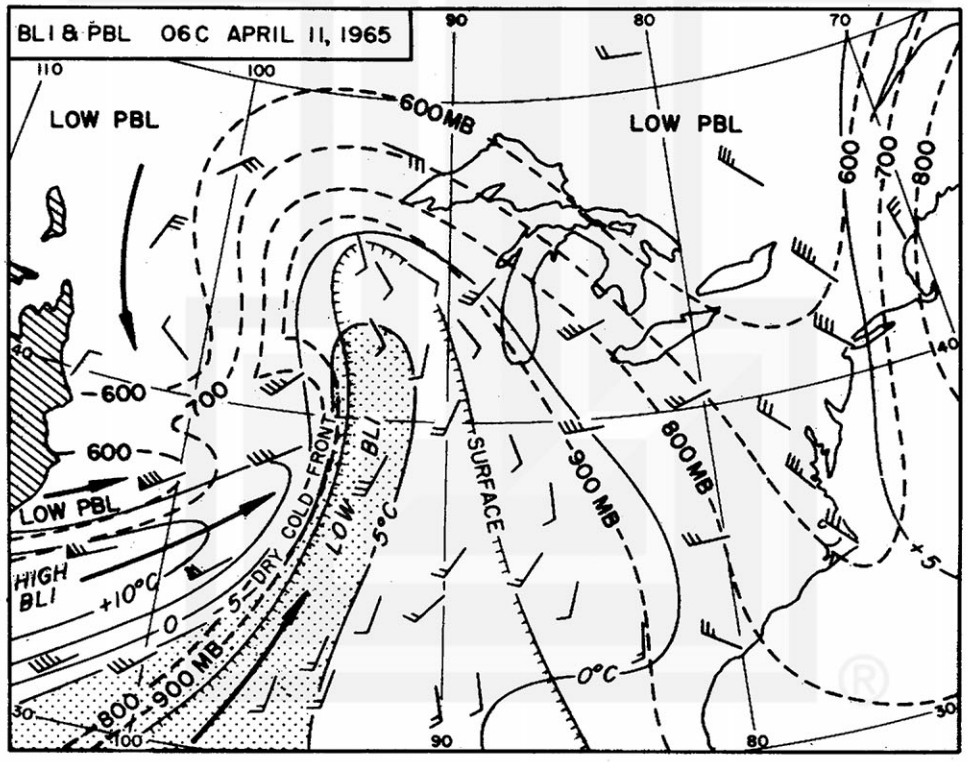

Figure 3. Isobars of PBL are represented by dashed lines and isolines of BLI by light solid lines. Area enclosed by line labeled "surface" indicates PBL is identical to pressure at the ground and the stippled area indicates BLI less than -5C. Plotted winds are those reported at or near the PBL surface. Heavy arrows represent the streamlines of the plotted winds.

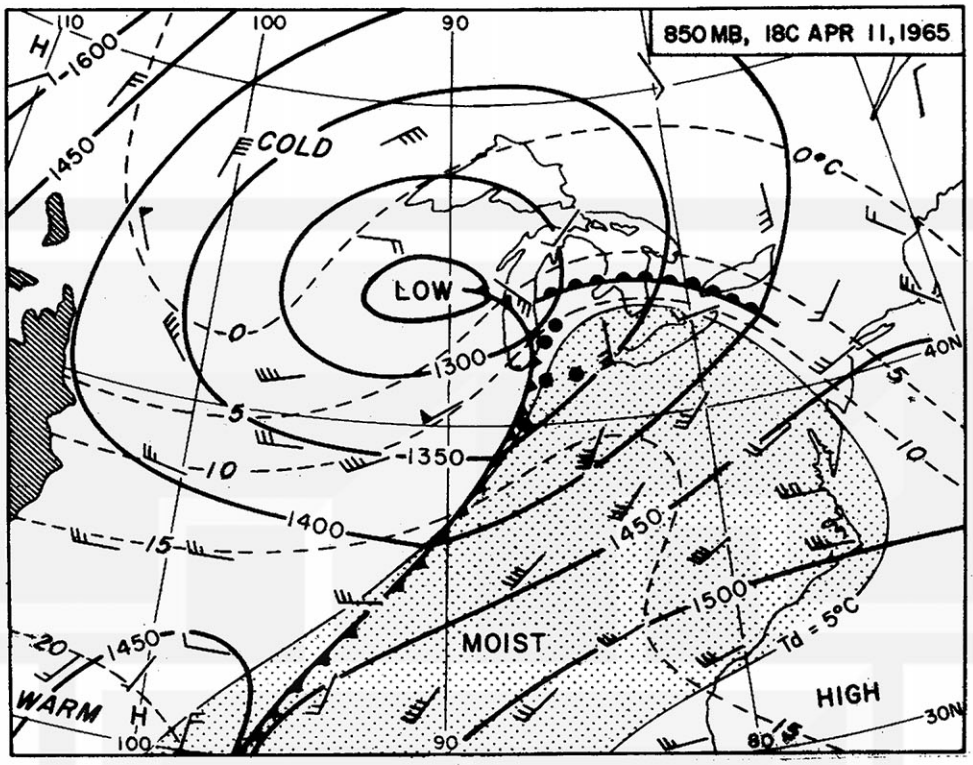

Figure 4. Fronts, contours (solid lines), and isotherms (dashed lines) on the 850-mb surface for 18 CST 11 April 1965. Stippled area represents dewpoint temperatures above 5C.

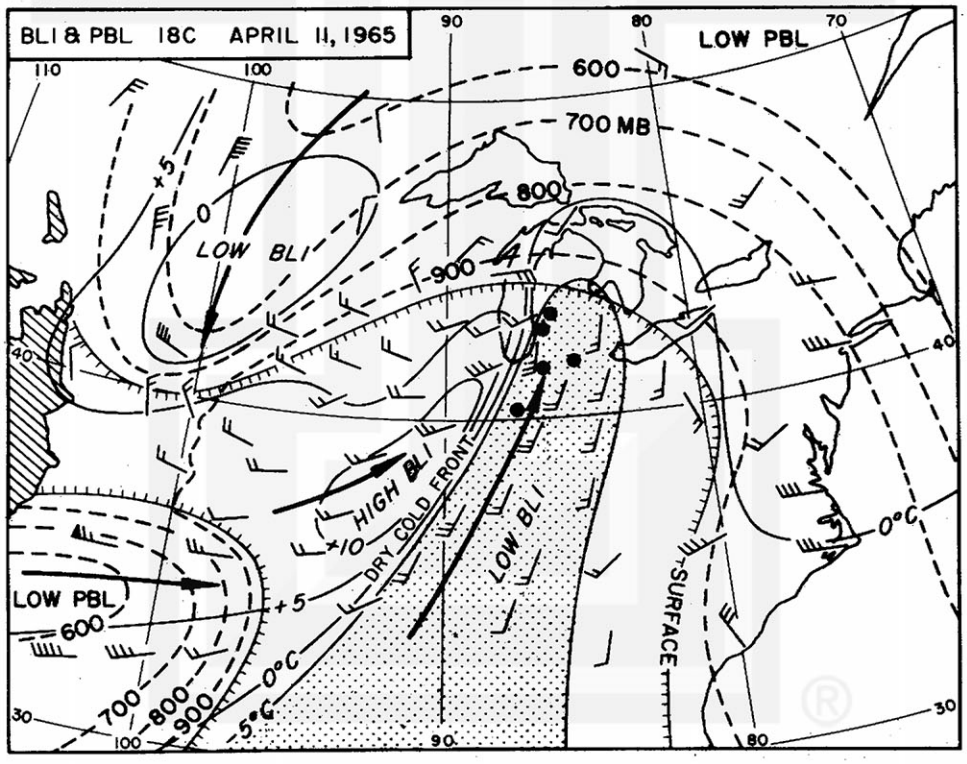

Figure 5. Isobars of PBL are represented by dashed lines and isolines of BLI by light solid lines. Area enclosed by line labeled "surface" indicates PBL is identical to pressure at the ground and the stippled area indicates BLI less than -5C. Plotted winds are those reported at or near the PBL surface. Heavy arrows represent the streamlines of the plotted winds. Black circles show position of tornadoes at 18 CST.

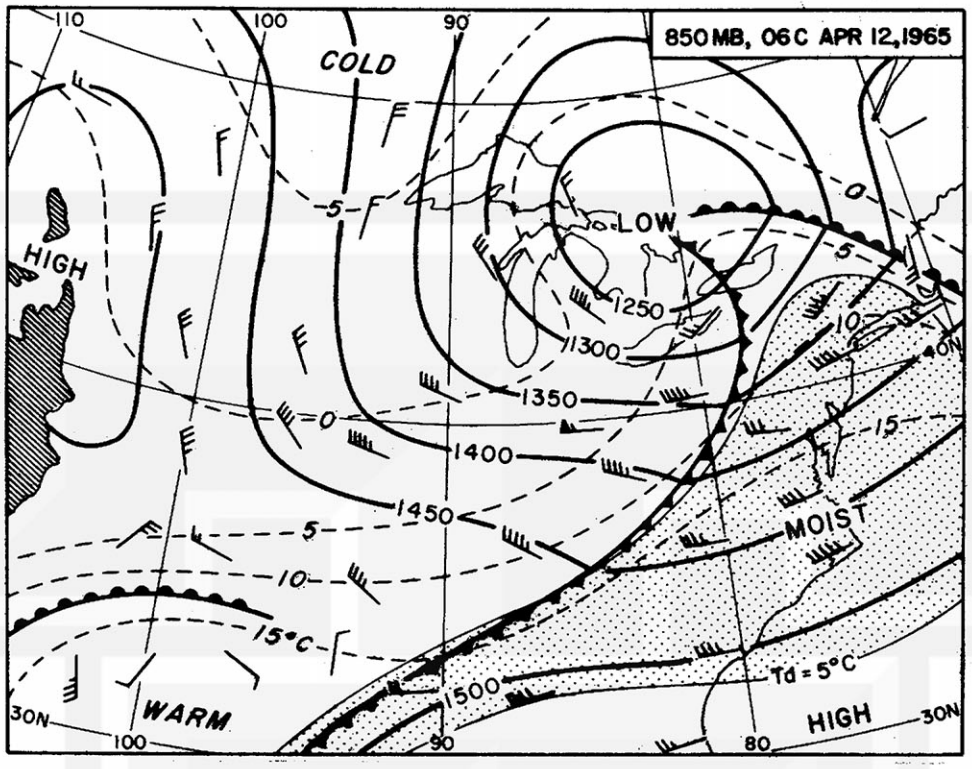

Figure 6. Fronts, contours (solid lines), and isotherms (dashed lines) on the 850-mb surface for 06 CST 12 April 1965. Stippled area represents dewpoint temperatures above 5C.

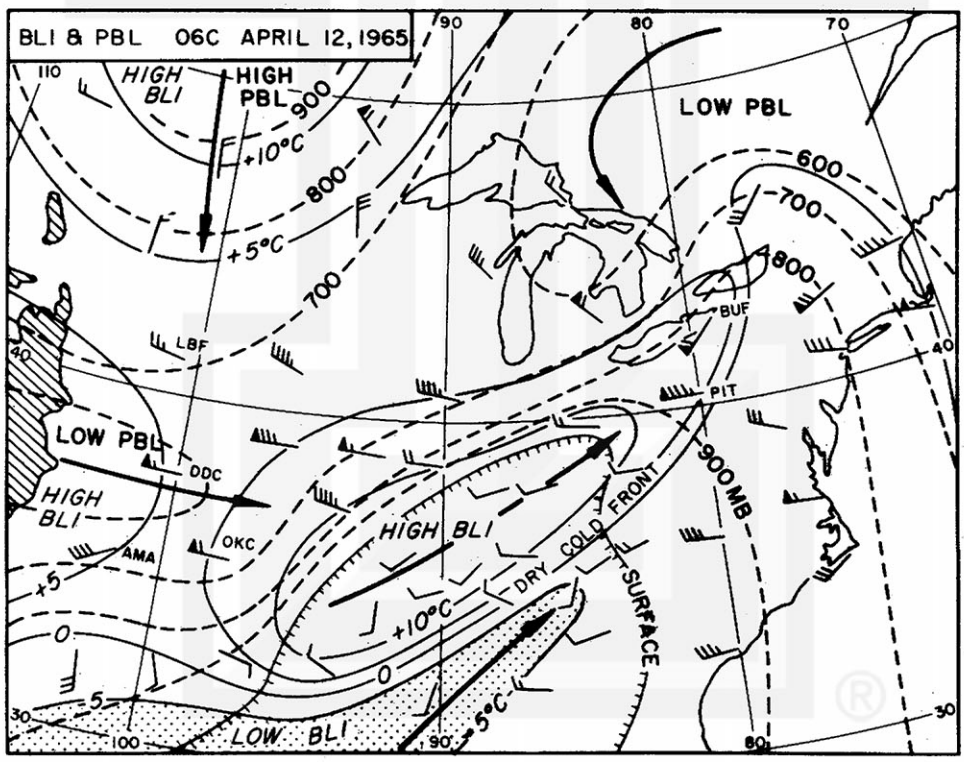

Figure 7. Isobars of PBL are represented by dashed lines and isolines of BLI by light solid lines. Area enclosed by line labeled "surface" indicates PBL is identical to pressure at the ground and the stippled area indicates BLI less than -5C. Plotted winds are those reported at or near the PBL surface. Heavy arrows represent the streamlines of the plotted winds.

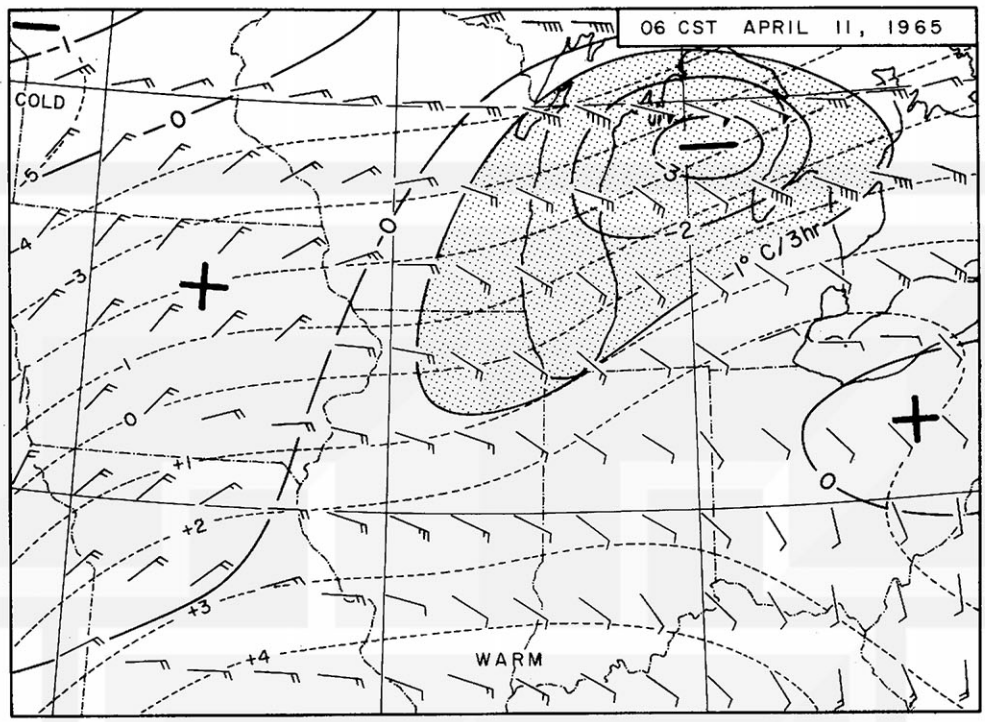

Figure 8. Chart showing isotherms (C) at 700-mb (dashed lines) and isolines of Material Differential Advection for low level winds (MDA-L) (solid lines) for 06 CST 11 April. Plotted winds at grid points are $V_{850}-V_{700}$.

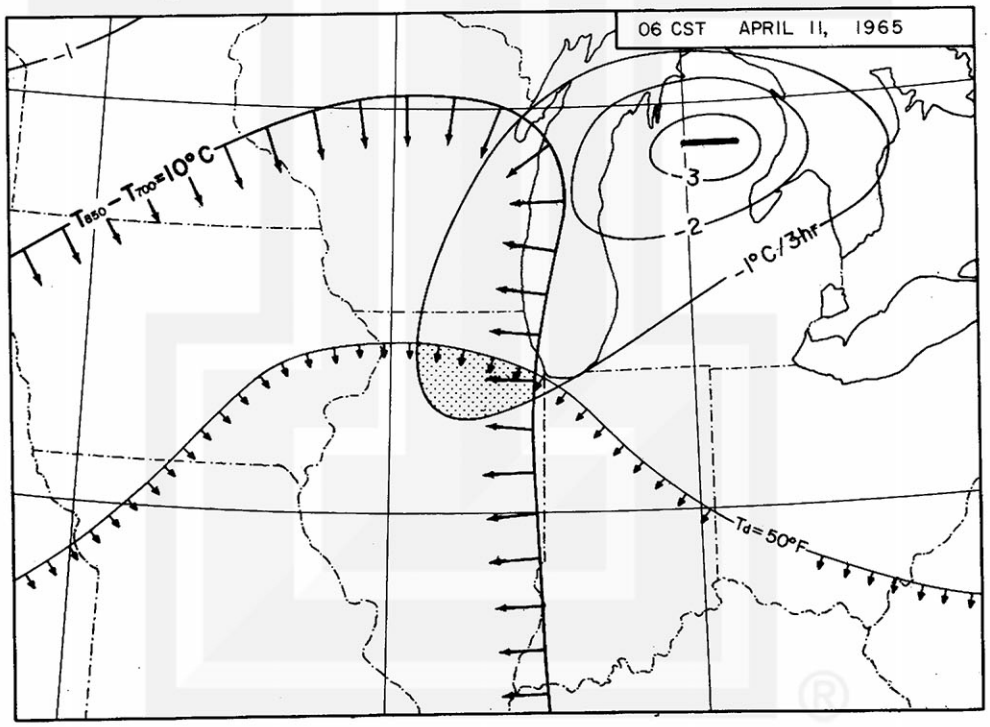

Figure 9. Chart showing MDA-L, in degrees C per 3 hours at 06 CST 11 April, combined with area in which temperature lapse between 850- and 700-mb is greater than 10C and with the area where the surface dewpoint is greater than 50F. The stippled area satisfies simultaneously the conditions of negative differential advection greater than 1C/3 hr, surface dewpoint greater than 50F, and a temperature lapse between 850- and 700-mb greater than 10C.

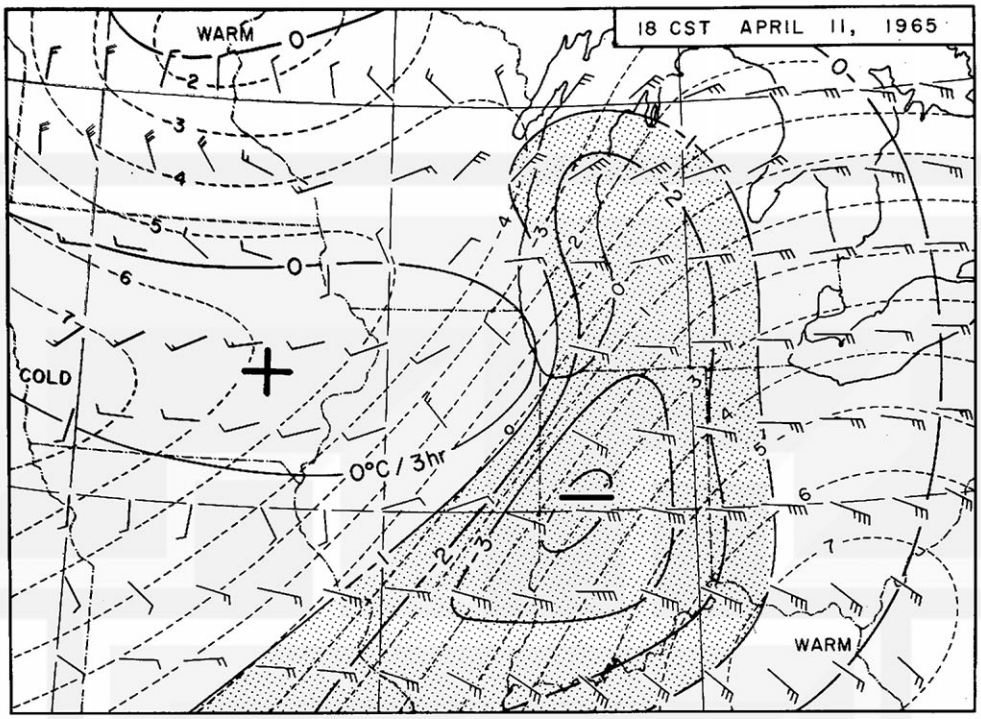

Figure 10. Chart showing isotherms (C) at 700-mb (dashed lines) and isolines of MDA-L (solid lines) for 18 CST 11 April 1965. Plotted winds at grid points are $V_{850} - V_{700}$.

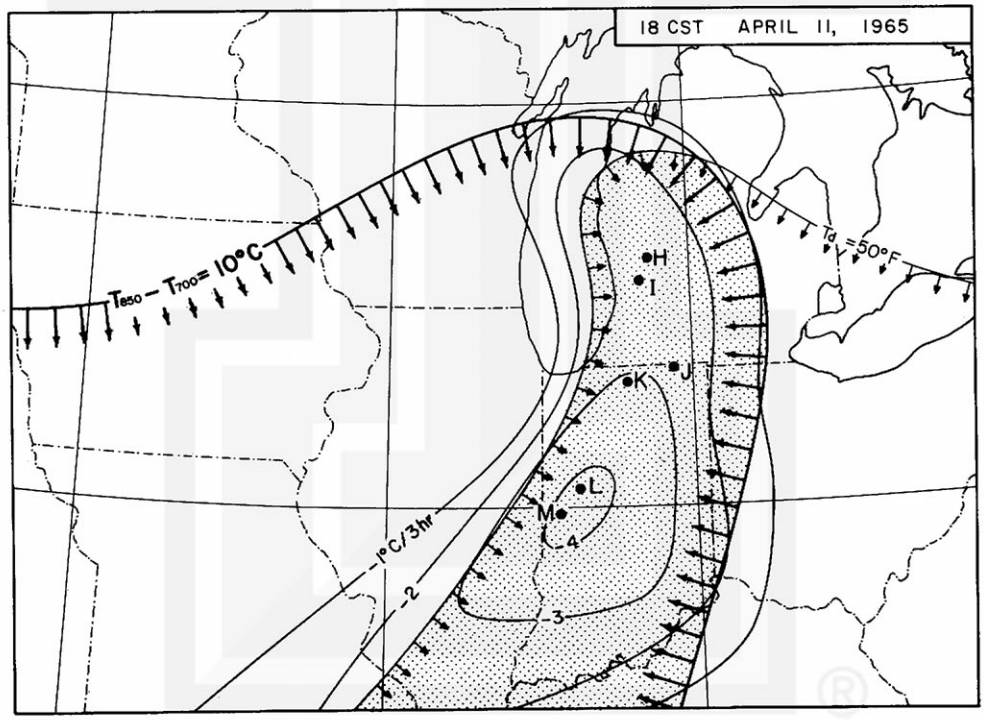

Figure 11. Chart showing MDA-L, in degrees C per 3 hours (at 18 CST 11 April, combined with the area in which temperature lapse between 850- and 700-mb is greater than 10C and with the area where the surface dewpoint is greater than 50F. The stippled area satisfies simultaneously the conditions of negative differential advection greater than 1C/3 hr, surface dewpoint greater than 50F, and a temperature lapse between 850- and 700-mb greater than 10C. Black circles represent location of tornadoes at chart time.

MESOMETEOROLOGY PROJECT - - - RESEARCH PAPERS

(Continued from front cover)

42. A Study of Factors Contributing to Dissipation of Energy in a Developing Cumulonimbus - Rodger A. Brown and Tetsuya Fujita

43. A Program for Computer Gridding of Satellite Photographs for Mesoscale Research - William D. Bonner

44. Comparison of Grassland Surface Temperatures Measured by TIROS VII and Airborne Radiometers under Clear Sky and Cirriform Cloud Conditions - Ronald M. Reap

45. Death Valley Temperature Analysis Utilizing Nimbus I Infrared Data and Ground-Based Measurements - Ronald M. Reap and Tetsuya Fujita

46. On the "Thunderstorm - High Controversy" - Rodger A. Brown

47. Application of Precise Fujita Method on Nimbus I Photo Gridding - Lt. Cmd. Ruben Nasta

48. A Proposed Method of Estimating Cloud-top Temperature, Cloud Cover, and Emissivity and Whiteness of Clouds from Short- and Long-wave Radiation Data Obtained by TIROS Scanning Radiometers - T. Fujita and H. Grandoso

49. Aerial Survey of the Palm Sunday Tornadoes of April 11, 1965 - Tetsuya Fujita

50. Early Stage of Tornado Development as Revealed by Satellite Photographs - Tetsuya Fujita

51. Features and Motions of Radar Echoes on Palm Sunday, 1965 - Dorothy L. Bradbury and Tetsuya Fujita